4 (2025) 100039

Contents lists available at ScienceDirect

Materials Chemistry and Physics: Sustainability and Energy

journal homepage: www.sciencedirect.com/journal/materials-chemistry-and-physics-sustainability-and-energy

Sintering inhibiting effect and enhanced CO_2 capture stability of MgO or La_2O_3 on calcined dolomite

Silvera Scaccia [a,*], Livia Della Seta [b], Daniele Mirabile Gattia [c]

[a] TERIN-DEC-CCT, V. Anguillarese 301, I-00123, Rome, Italy
[b] TERIN-DEC-H2V, V. Anguillarese 301, I-00123, Rome, Italy
[c] SSPT-PROMAS-MATPRO, C.R. ENEA, Casaccia, V. Anguillarese 301, I-00123, Rome, Italy

ARTICLE INFO

Keywords:
Dolomite
CO2 capture
Sintering
MgO
La2O3

ABSTRACT

The beneficial effect of 20 %wt.MgO or 20 %wt.La_2O_3 additives on pre-calcined dolomite to improve the CO_2 sorption capacity in the calcium looping cycle (CaL) was studied by TG/DTG/DSC techniques at carbonation temperatures of 600–700 °C under mild conditions (carbonation in 25 %CO_2–N_2 balance and calcination at 900 °C in pure N_2). The doped pre-calcined dolomites were prepared by wet chemical mixing method, followed by air-calcination at 900 °C, and characterized by XRD, SEM-EDS, and N_2-physisorption analysis. Doped calcined dolomite exhibited a noticeably reduction of CaO crystallite size and enhanced S_{BET}. In La_2O_3-doped calcined dolomite the formation of $La_2O_2CO_3$ after carbonation stage was clearly confirmed by DTG/XRD analysis. After 10th CaL cycles both doped calcined dolomites showed minor deactivation degree and higher cycling stability over 40th CaL cycles compared to undoped dolomite. Kinetics analysis by the classical grain model estimated the intrinsic specific rates (k) in the kinetic-controlled stage significantly higher for the MgO doped calcined dolomite. Meanwhile the Arrhenius activation energy values of 18.1 and 24.6 kJ mol^{-1} and pre-exponential factors of $4.5{\cdot}10^{-3}$ and $5.6{\cdot}10^{-3}$ mol m^{-2} s^{-1} for MgO and La_2O_3 additives, respectively, were lower compared to undoped calcined dolomite (E_a = 35.1 kJ mol^{-1} and A = $0.15{\cdot}10^{-3}$ mol m^{-2} s^{-1}).

1. Introduction

In recent decades, the CaO/$CaCO_3$ system has gained considerable attention due to its use as solid sorbent for CO_2 capture in advanced environmentally friendly and energy-saving technologies [1,2]. In particular, Calcium Looping (CaL), a process of repeated carbonation-calcination cycles of CaO-based sorbents in dual fluidized reactor, is a promising technology to be applied in various processes for CO_2 capture in pre-and- post combustion (CaL-CCS), thermochemical energy storage (CaL-TCES), and in intensive reforming processes like dry reforming of methane (CaL-DRM) and steam reforming of methane (CaL-SRM) [3–6]. However, the poor stability of CaO-based sorbents over multiple cycles, which depends on a series of intrinsic and extrinsic features, severely restricted CaL process application. Therefore, it is essential to direct the research efforts to avoid the rapid decay of CaO-based sorbent activity and make it suitable for long-term use.

The CO_2 capture capacity of CaO is based on the following reversible reaction [7]:

$$CaO_{(s)} + CO_{2(g)} \rightleftarrows CaCO_{3(s)} \quad (1)$$

where the CaO solid can accept CO_2 gas through an exothermic reaction ($\Delta H^0_{298K} = -178$ kJmol^{-1}) thermodynamically favored at low temperature, whereas calcination produces solid CaO and CO_2 evolution through an endothermic process ($\Delta H^0_{298K} = +178$ kJmol^{-1}) thermodynamically favored at high temperature. However, the reversibility of the two above-mentioned reactions is not completely achieved owing to the sintering phenomenon (Tammann temperature of $CaCO_3 \approx 530$ °C) during the calcination stage. Therefore, under realistic conditions a decay of CO_2 capture capacity of CaO among cycles has been often experienced [8]. Many efforts have been made to alleviate the loss of CO_2 capture capacity of CaO, including thermal treatments [9], chemical treatments [10], lowering the calcination temperature [11], and incorporation of an inert material into the structure of CaO [12], and many breakthroughs have been achieved. However, despite the extensive research conducted so far, further investigations are needed before it can be used on an industrial scale [13].

Naturally occurring minerals such as limestone and dolomite (a

* Corresponding author.
E-mail address: silvera.scaccia@enea.it (S. Scaccia).

https://doi.org/10.1016/j.macse.2025.100039
Received 13 February 2025; Received in revised form 31 July 2025; Accepted 5 August 2025
Available online 7 August 2025

double salt of magnesium and calcium carbonate) can provide very cost-effective metal oxide CaO owing to their abundance. Although the theoretical CO_2 capture capacity of lime CaO (0.786 g CO_2/g CaO) is higher than that of calcined dolomite due to the presence of large amounts of $MgCO_3$ in natural dolomite, the absorption performance of CaO-derived dolomite at different temperatures was found to be optimal because it had shorter absorption times and higher CO_2 adsorption potential than limestone-based sorbents [14,15]. The presence of MgO in calcined dolomite is beneficial because, acting as an inert material with high Tammann temperature (1563 °C, [16]), it can stabilize the particles morphology by slowing down the grain growth of particles [17]. Based upon this ascertainment, the addition of MgO to inhibit the sintering effect of CaO grains has been widely investigated in the last two decades [18–20]. Doping CaO with 20 wt% MgO exhibited 45 % greater absorption capacity than undoped CaO and higher stability after 1250 carbonation/calcination cycles [21]. Synthetic Ca-rich dolomites were prepared by mixing Ca^{2+} and Mg^{2+} at molecular level as in natural dolomite to increase the stability over cycles because the presence of inert component at macroscopic level is not alone sufficient to stabilize pore structure [22]. By using calcium and magnesium salts of D-gluconic acid through an aqueous solution precipitation technique fine CaO sorbent particles were formed with adhering MgO nanoparticles on its surface, which acting as physical barrier could prevent sintering and agglomeration of CaO particles [23]. However, a higher content of MgO incorporated into the CaO matrix led to a better cyclability at expense of lower absolute CO_2 capture capacity [23,24].

To improve the CO_2 capturing capability of dolomite-derived sorbents various modifications were experienced such as carbon coating [25] and doping with foreign elements such as alkali metal salt, Ni, Fe, Mn, Zr, Ce, and La [26–30]. Lanthanum trioxide, having high melting point and basic properties, has been proposed as inert material to highly disperse CaO sorbent particles and avoid particles agglomeration and sintering [31]. Indeed, it was found that Ca^{2+} and La^{3+} having similar ionic radii their mutual substitution into CaO and La_2O_3 matrices may produce oxygen vacancies and more suitable surface properties. The basic properties of the rare-earth element La tend to neutralize the acidic gas (CO_2) and enhance the CO_2 absorption capacity on CaO [32]. Even more, La_2O_3 can be a CO_2 acceptor through the formation of $La_2O_2CO_3$, the stable intermediate in the decomposition of lanthanum carbonate, which decomposes above 720 °C, depending on partial pressure of CO_2 in the gas phase, as follows [33]:

$$La_2O_2CO_3 \rightleftarrows La_2O_3 + CO_2 \quad (2)$$

It was hypothesized that the carbonation reaction of La_2O_3 present in the matrix of CaO could occur during the carbonation/calcination reactions at 750 °C since small amounts of $La_2O_2CO_3$ were detected by XRD in the CaO/La_2O_3 mixtures subjected to repeated carbonation/calcination cycles [21]. This event could be responsible for the significant improvement of the sorbent stability during CO_2 capture observed up to 30 CaL cycles. Unfortunately, this positive effect disappeared with increasing cycles number. To verify this, pure La_2O_3 was subjected to four CaL cycles and the adsorbed CO_2 was only 0.1•10-3 mol of CO_2 per gram of sorbent. It is plausible that the low regeneration temperature does not allow the complete decarbonization of $La_2O_2CO_3$. Furthermore, the $La_2O_2CO_3$ formed during the carbonation stage could not be completely decomposed under realistic 100 % CO_2 atmosphere regeneration conditions due to the equilibrium pressure of CO_2 according to eq. (2) and might contribute partially to CO_2 capture, whereas La_2O_3/-$La_2O_2CO_3$ can act as a barrier against sintering [30].

The effectiveness of modification of natural dolomite by doping with foreign elements mostly depends on the sorbent preparation methods like coprecipitation [34], ball-milling [35], dry and wet physical mixing [36,37], sol-gel/wet impregnation [38]. Wet chemical methods are designed to allow inert materials to act effectively as a barrier between CaO particles rather than through mechanical mixing. However, the application of the CaL process to friendly renewable energy sources or the modernization of existing coal-fired plants will depend on the cost-effective approach in improving the multicycle stability of CaO [39].

In this work, pre-calcined dolomite doped with 20 %wt. MgO or 20 % wt. La_2O_3 was studied to understand the anti-sintering ability of excess MgO or to highlight the beneficial effect of La_2O_3 by capturing extra CO_2 or by reducing the agglomeration effect during calcination. The doped pre-calcined dolomites were prepared by wet chemical mixing method and characterized by XRD, SEM, and N_2-physisorption analysis. The effect of adding metal oxides to pre-calcined dolomite on CO_2 capture capacity was investigated by TG/DTG/DSC techniques under CaL conditions. Kinetic analysis was also conducted by the classical grain model for non-catalytic gas-solid reactions to calculate intrinsic specific rate constants and as well energy of activation and pre-exponential factor.

2. Experimental

2.1. Instrumentations

Powder X-ray diffraction (XRD) patterns of samples were recorded on a SmartLab Rigaku X-Ray diffractometer using Ni filtered Cu Ka (1.5406 Å) radiation operating at 40 kV and 30 mA. The measurements were taken over Bragg angle (2θ) every 0.02° ranging from 5 to 90° at scan rate of 2° min^{-1}. The diffraction patterns were matched with those of International Centre for Diffraction Data (ICDD) database. The average crystallite sizes of samples were calculated using Scherrer's equation [40]:

$$D_{XRD} = 0.9\lambda/\beta \cos\theta \max \quad (3)$$

where D_{XRD} is the crystallite size in nm, λ the radiation wavelength (Cu Kα radiation 0.15406 nm), β the bandwidth at half-height, and θ is the diffraction peak angle.

X-ray fluorescence (PANalytical Epsilon 5) was used for qualitative and quantitative analysis of inorganic compounds in natural dolomite.

FTIR spectrometer (Varian 640) was used for the analysis of calcined dolomite with KBr method. The FTIR spectrum was recorded by co-adding 20 scans in the 4000-400 cm^{-1} region at a resolution of 2 cm^{-1}. The assignments of IR absorption bands were based on the work of [41].

The morphology and the dimensions of samples were observed by scanning electron microscope (Vega 3 Tescan) equipped with an Element Energy Dispersive Spectroscopy (EDS) System EDAX for elemental mapping analysis. Prior to analysis, the powdered samples were sputtered-coated with graphite with the aim of increase the sample conductivity for scanning.

The specific surface area (S_{BET}) and BJH total pore volume of fresh sorbents and after CaL test were measured using a Micromeritics TriStar 3000 V6.04 instrument and the measurements were based on the Brunauer-Emmett-Teller (BET) method [42]. N_2 adsorption-desorption isotherms were obtained using a nitrogen bath at −196 °C. Prior measurements, the samples were degassed at 120 °C for 2 h.

Thermogravimetric analyzer (TGA/DSC1 STARe System, Mettler-Toledo, Switzerland) equipped with a flow gas control system was used. Nitrogen (99.99 %, Air Liquid, France) was used as the purge gas at 0.030 L min^{-1} to protect the balance. Synthetic air and CO_2 (99.99 %, Air Liquid, France) were used. The total flow rate was 0.110 L·min^{-1}. Typical sample mass of 0.010 g was placed in an open cylindrical alumina crucible (0.03•10^{-3} L) and heated at 10 °C·min^{-1} heating rate up to 1000 °C under dynamic synthetic air otherwise stated. Blank correction runs were carried out to minimize the Buoyancy effect.

2.2. Chemicals and material

MgO and $La(OH)_3$ of analytical grade (99.7 %) from Merck were

dried at 120 °C for 2 h. 2-propanol (reagent grade, 99.8 %) was from Merck. Pure La_2O_3 was obtained by calcining $La(OH)_3$ precursor at 900 °C in air for 2 h. De-ionized water (18.0 MΩ cm conductivity) was used throughout the experiments. Natural dolomite was from quarry of Biella (Italy). The as-received dolomite, supplied in powder form, was homogenized by hand grinding in an agate mortar and sieved to produce a sample with a grain size below 1.5 mm. The as-grinded dolomite was characterized by various techniques and the results are described below.

2.3. Dolomite characterization

The XRD pattern shown in Fig. 1a confirmed the presence of dolomite (PDF: 00-005-0622) and some free calcite (PDF: 01-083-1762). Meanwhile the FTIR spectrum in Fig. 1b showed the presence of both

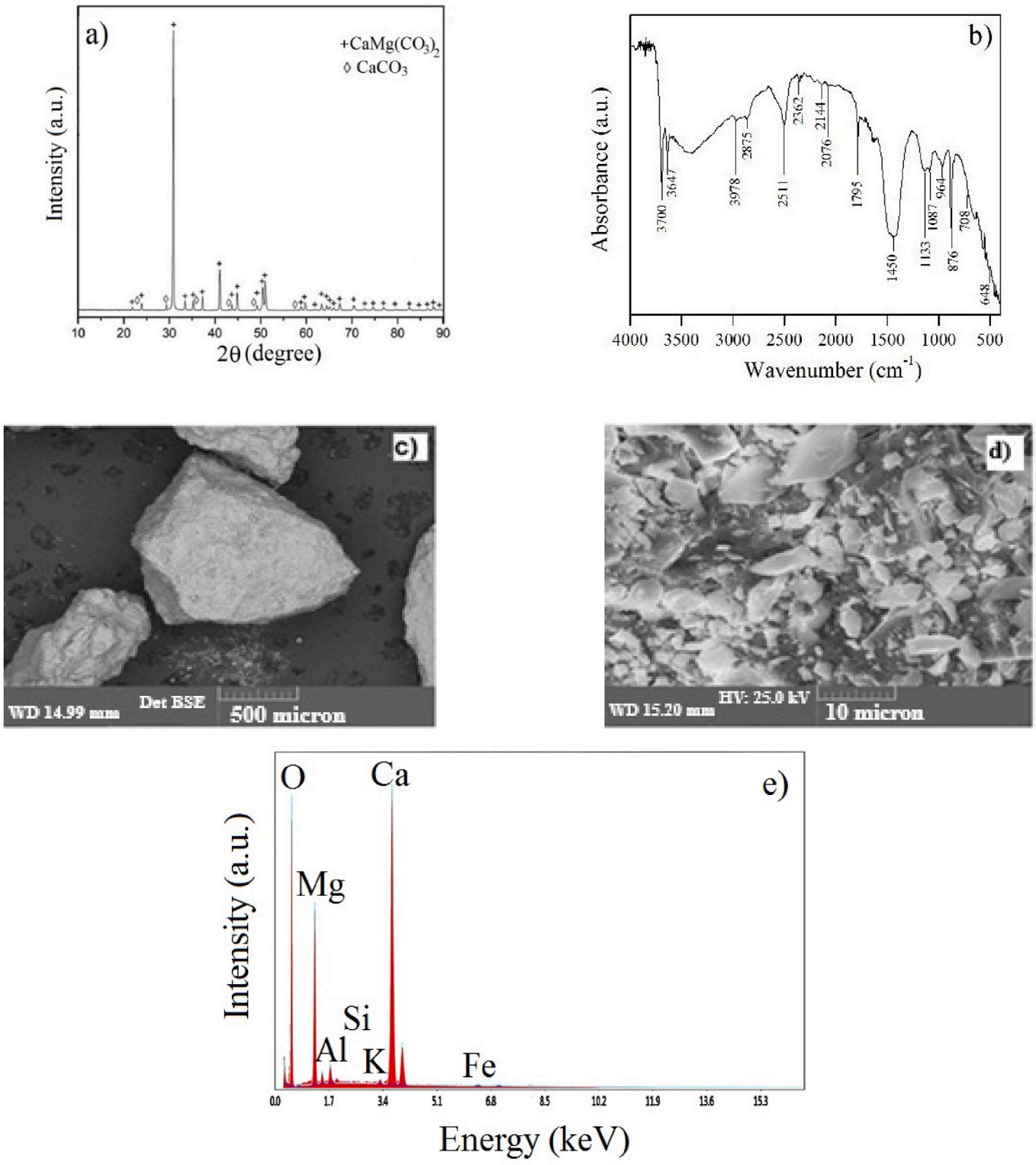

Fig. 1. Results of characterization of as-grinded dolomite: XRD pattern (a); FTIR spectrum (b); selected representative backscatter (c) and SEM (d) images along with the corresponding EDS spectrum (e).

$Mg(OH)_2$ and $Ca(OH)_2$ (peaks at 3700 and 3647 cm^{-1} due to O-H stretching of hydroxyl group, respectively) [43]. The SEM images by back-scattered electron signal (Fig. 1c) and secondary electron signal (Fig. 1d) showed that the surface morphology of granules was composed by flat platelets. It was computed by qualitative SEM-EDX analysis the presence in virgin dolomite, other than obvious Ca and Mg, impurities such as K, Al, Fe, and Si (Fig. 1e). X-ray fluorescence analysis gave quantitative results as reported in Table 1.

Thermal analysis of as-grinded dolomite was conducted in the temperature range ambient-1000 °C at 10 °C·min^{-1} heating rate under both 80 % (v/v) CO_2 and air atmospheres and the results are showed in Fig. 2. The TG curve under CO_2 atmosphere shows one mass loss of about 2 % starting at 450 °C, which was due to decomposition of free $Mg(OH)_2$/$Ca(OH)_2$ to MgO/CaO. Two main well defined mass losses were observed at temperature above 600 °C, which were accompanied by the corresponding two endothermic effects at 763 °C and 917 °C, each corresponding to approximately to half of the CO_2 content of the mineral providing magnesium and calcium oxides in two successive steps as follows [44]:

$$\begin{aligned} &CaMg(CO_3)_{2\backslash(s)}I \\ &\rightarrow Ca(CO_3)MgO_{(s)} + CO_{2(g)}II \\ &\rightarrow MgO_{(s)} + CaO_{(s)} + CO_{2(g)} \end{aligned} \quad (4)$$

The TG profile of natural dolomite under fluxing air showed a single mass loss step of about 46.5 %, which was accompanied by an endothermic peak at 763 °C [45]. The residual mass at the end of each run was considered to be the pre-calcined dolomite, which was constituted by MgO and CaO and plus other impurities. Therefore, based on TGA results the pre-calcined dolomite was mainly composed by 30.2 %wt. CaO and 20.7 %wt. MgO and the mass fraction of CaO and MgO were $f_{CaO} = 30.2/52.4 = 0.58$ and $f_{MgO} = 20.7/52.4 = 0.40$. Accordingly, the theoretical maximum CO_2 uptake capacity of pre-calcined dolomite can be calculated as 0.452 $g_{CO_2}{\cdot}g_{sorbent}{}^{-1}$.

2.4. Preparation of calcined dolomite and doped calcined dolomite

The as-grinded dolomite was calcined in a horizontal electric furnace at 900 °C with heating rate of 10 °C·min^{-1} in static air for 2 h. The pre-calcined dolomite was hereafter referred to calc-DOL. The pre-calcined dolomite was doped with 20 %wt. MgO or 20 %wt. La_2O_3 (using $La(OH)_3$ as precursor) by a wet chemical mixing method as schematically illustrated in Fig. 3. Firstly, 1 g of fresh pre-calcined dolomite was transferred to a covered quartz flask containing 20 mL of deionized water/2-propanol (1 + 1 v/v) mixture and held under refluxing at 80 °C with vigorous magnetic stirring for 2 h. Afterwards MgO or La_2O_3 was added to the slurry in a mass ratio pre-calcined dolomite to dopant of 4 to 1 and constantly held under stirring for 2 h. Specifically, 0.25 g of MgO or 0.29 g $La(OH)_3$ were accurately weighed and added to the slurry. Then, the solvent was left to slowly evaporate in a heating mantle at 150 °C overnight. Finally, the sample was transferred to an alumina boat, which was introduced in a horizontal electric furnace and thermally treated at 900 °C at heating rate of 10 °C·min^{-1} in air for 2 h. The obtained samples were cooling down at room temperature and immediately stored in a desiccator to avoid moisture and CO_2 contamination from the atmosphere. Based on stoichiometry the mass fraction of CaO in the doped sorbent was f_{CaO} = 0.48. Accordingly, the theoretical maximum CO_2 uptake capacity of doped calcined dolomite can be calculated as 0.38 $g_{CO_2}{\cdot}g_{sorbent}{}^{-1}$. The pre-calcined dolomite samples added with 20 %wt. MgO or 20 %wt. La_2O_3 additives were referred to MgO-calc-DOL, and LaO-calc-DOL, respectively.

Table 1
XRF elemental composition analysis of as-grinded dolomite (wt.%).

Sample	Ca	Mg	K	Al	Fe	Si
As-grinded dolomite	21.7	12.6	0.1	0.2	0.5	0.3

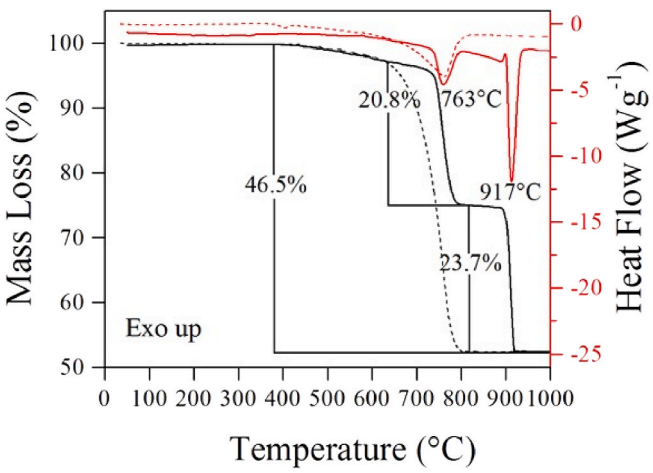

Fig. 2. Thermal decomposition of as-grinded dolomite by TG-DSC at 10 °C·min^{-1} under both 80 % (v/v) CO_2 (–) and air (–) atmospheres.

2.5. Calcium looping (CaL) cycles

The CaL cycles were carried out in a thermogravimetric analyzer (TGA/DSC1 STARe System) equipped with a cooling water circulator. Typical sample mass was 0.010 g (or 0.1 g for BET spent analysis) and placed in an open cylindrical alumina crucible (70·10^{-6} L). An empty alumina crucible was used as reference. Nitrogen at 0.030 L·min^{-1} was used as the purge gas to protect the balance. The following thermal program was used: at first the samples were heated at 50 °C·min^{-1} from ambient temperature to 900 °C under 100 % (v/v) N_2 at 0.060 L·min^{-1} total flow rate (carrier + purge) and maintained at this temperature for 10 min. Then, the samples were cooled down at to 600, 650 or 700 °C at 10 °C·min^{-1} under 100 % (v/v) N_2 at 0.060 L·min^{-1} total flow rate and kept isothermally at the given temperature for 5 min. After that, the CO_2 reactant gas at 0.020 L·min^{-1} flow rate was introduced in the carrier gas. The total flow rate was 0.080 L·min^{-1}. The carbonation step was performed for 30 min in 25 % (v/v) CO_2 to evaluate the rate of the diffusion reaction and the calcination step was performed at 900 °C in 100 % (v/v) N_2 for 30 min. The looping cycle (carbonation-calcination reactions) was controlled by the software Relative Loop. Long term test to evaluate the sorbent performance comprised 40 CaL cycles. The CO_2 uptake capacity, *C*, and conversion, X, of sorbent was expressed as follows:

$$C = \frac{m_f - m_0}{m_0}\left(g_{co_2} \cdot g_{sorbent}{}^{-1}\right) \quad (5)$$

$$X = \frac{(m_f - m_0)M_{CaO}}{m_0 f_{CaO} M_{CO_2}} \quad (6)$$

Where m_f is the sample mass at the end of each carbonation cycle, m_0 is the initial sample mass, f_{CaO} is the active mass CaO fraction in the samples, and M_{CaO} and M_{CO_2} are the molecular weights of CaO and CO_2, respectively.

3. Results and discussion

3.1. Characterization of undoped and doped calcined dolomite

The XRD patterns of the freshly calc-DOL, as-prepared MgO-calc-DOL and as-prepared LaO-calc-DOL sorbents are shown in Fig. 4. From Fig. 4 the diffraction peaks belonging to MgO (PDF 45–946) and CaO (PDF: 01-083-1762) phases were distinctly identified in all three samples. No diffraction peak belonging to dolomite was detected, indicating complete de-carbonation of dolomite under the given calcination

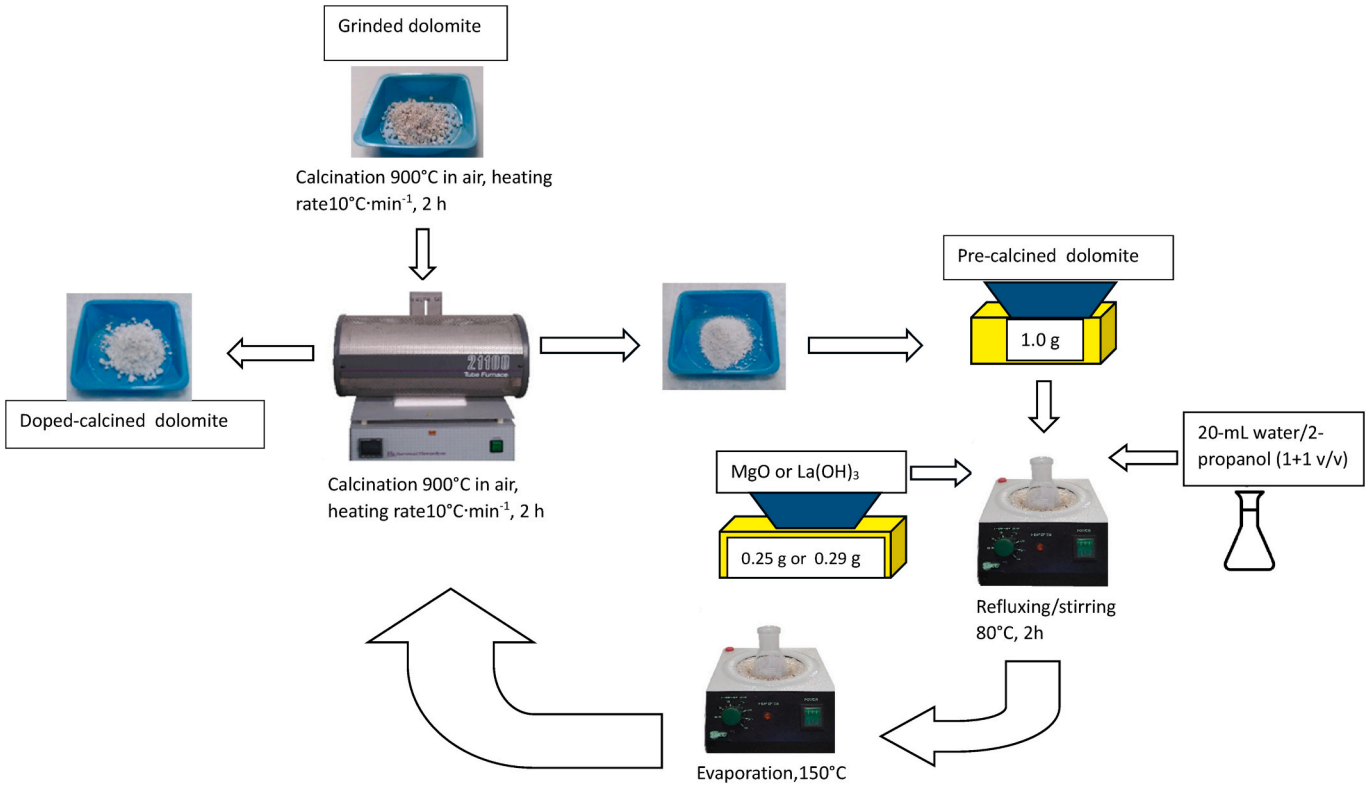

Fig. 3. Schematic illustration of preparation method for doped-calcined dolomite.

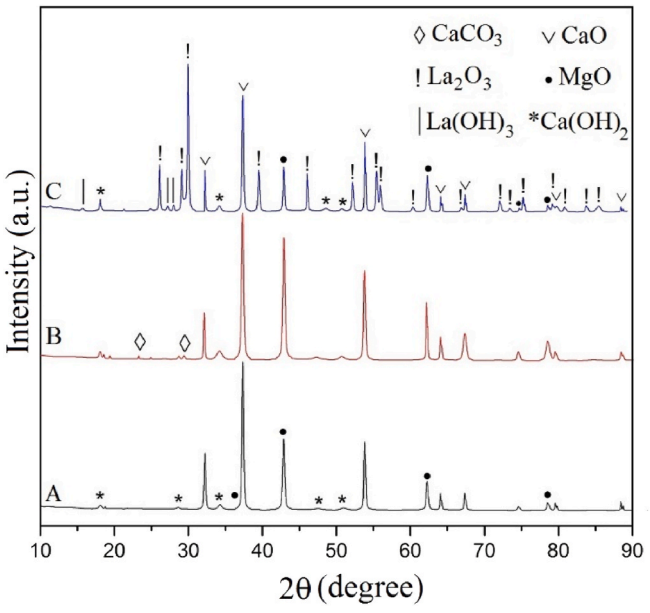

Fig. 4. XRD patterns of: (A) freshly calc-DOL, and as-prepared (B) MgO-calc-DOL and (C) LaO-calc-DOL.

conditions in accordance with the TG results. Some small extra peaks ascribed to $Ca(OH)_2$ and $CaCO_3$ were due to the high sensitivity of CaO to moisture and ambient carbon dioxide. For the calcined dolomite doped with $La(OH)_3$ precursor, well-defined diffraction peaks belonging to the newly formed hexagonal phase La_2O_3 (PDF-05–0602) were evidenced in the XRD pattern of the as-prepared LaO-calc-DOL sample along with small amount of $La(OH)_3$ coming from air exposure contaminations (Fig. 4C). XRD analysis performed on samples quenched from 600 to 700 °C carbonation temperature after exposure to 25 % CO_2–N_2 balance for 30 min during the first CaL cycle showed that the results were similar each other and, for brevity, those obtained at 700 °C are displayed in Fig. 5(A-C). As expected, the newly formed calcium carbonate crystal phase was detected in all three samples along with trace of un-carbonated CaO and unreacted MgO. An exception is made for the LaO-calc-DOL sample, which showed well-resolved diffraction

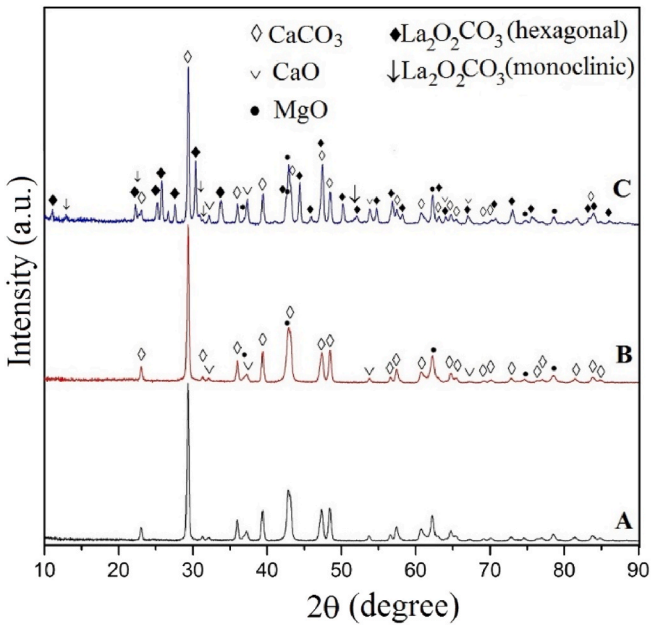

Fig. 5. XRD patterns of: (A) calc-DOL, (B) MgO-calc-DOL, and (C) LaO-calc-DOL after carbonation step of the 1st CaL cycle at 700 °C under 25 % CO_2 (N_2 balance).

peaks at 2ϑ between 25-28° and 30–35° indexed to the hexagonal form of $La_2O_2CO_3$ (PDF-48-1113) along with that of its monoclinic polymorph. Meanwhile no trace of La_2O_3 was detected. From XRD analysis it was well-evident that after the first exposition of LaO-calc-DOL to CO_2 adsorption, the La_2O_3-dopant undergoes to carbonation reaction forming bulk lanthanum oxy carbonate. In order to insight whether $La_2O_2CO_3$ decomposes into La_2O_3 during calcination at 900 °C under N_2, XRD analysis (not shown here) of the LaO-calc-DOL sorbent submitted to the first CaL cycle and stopped after the calcination step showed mainly diffraction peaks belonging to the La_2O_3 phase.

The crystallite size (D_{XRD}) of CaO particles for various freshly prepared sorbents was calculated from the XRD patterns above presented using the diffraction peak at $2\vartheta = 31.45°$ corresponding to the (111) diffraction plane through Scherrer equation. A significant decrease in the CaO crystal size by incorporation of extra 20 wt % MgO or doping with 20 wt % La_2O_3 in pre-calcined dolomite structure by approximately 26 % (D_{XRD} = 28.9 nm) and 15 % (D_{XRD} = 33.3 nm), respectively, compared to unmodified calcined dolomite (D_{XRD} = 39.0 nm) was observed. These results are consistent with literature data [46] and confirm that additional doping metals controlling the CaO grain size in calcined dolomite could be beneficial for the CO_2-CaO gas-solid reaction.

Some physical properties, such as S_{BET} and BJH pore volume, of all the three fresh sorbents along with the raw dolomite are reported in Table 2. After 40th CaL cycles the sorbents were re-analyzed and the results are also reported in Table 2. As it can be seen, the raw dolomite presents BET surface area and pore volume values typical of non-porous materials. After calcination of the raw dolomite at a relatively high temperature of 900 °C in air the calcined dolomite had a higher S_{BET} of 20.0 $m^2\ g^{-1}$ and BJH total pore volume of 0.148 $cm^3\ g^{-1}$, values in good agreement with literature data [47]. During complete thermal decomposition, virgin non-porous dolomite transforms into a highly porous material, which depends on the partial pressure of CO_2 and temperature conditions. Thus, through such porosity the CO_2 gas reaches the CaO particles to be absorbed, even though CO_2 accumulation plays a prominent role in sintering and swilling process [48]. From Table 2 it is seen the S_{BET} values of fresh doped calcined dolomites were increased of about 27 and 25 % for MgO-calc-DOL or LaO-calc-DOL, respectively, compared to undoped calcined dolomite. It is supposed that the addition of MgO and La_2O_3 coming from $La(OH)_3$ decomposition can play a fundamental role in improving the BET specific surface area. However, the loss-in-S_{BET} and BJH pore volume was revealed for both doped and undoped calcined dolomite subjected to a series of 40 CaL cycles in TGA (see Table 2). The lower values were found for the undoped calcine dolomite as consequence of severe sintering and collapse of pores compared to doped calcined dolomites. This result is consistent with the SEM analysis, as it will be discussed below. The good texture shown here by the spent doped dolomites should favor a higher CO_2 capture capacity.

Morphological characterization of freshly calcined dolomite and doped calcined dolomite after 40th CaL cycle was conducted by SEM-EDS analysis. The SEM image of freshly pre-calcined dolomite reported in Fig. 6a(A) showed a uniform nano-crystal structure composed of small spherical grains with sizes ranging from 100 to 500 nm, which gives rise to roughness and porous surface compared to its dense surface original morphology (see Fig. 1c,d) as a consequence of CO_2 evolution during the dolomite thermal decomposition. The addition of MgO or La_2O_3 to pre-calcined dolomite revealed no obvious morphological changes of the homogenous dispersion of small spherical crystallites, but the particle size was noticeably reduced (Fig. 6a(B-C)). A representative SEM-EDS image/spectrum of as-prepared LaO-calc-DOL is showed in Fig. 6b. Qualitative EDS mapping of Ca, Mg and La elements confirmed uniform lanthanum metal distribution within the CaO·MgO matrix indicating the good reliability of the doped sorbent preparation method. For simplicity, in Fig. 7 are depicted SEM images of spent undoped and doped calcined dolomites subjected to cycling at 700 °C carbonation temperature. The SEM image of the spent undoped calcined dolomite revealed substantial adhesion among dolomitic grains forming dense agglomerates so destroying the porous structure (Fig. 7A). On the contrary the spent doped calcined dolomites possessed still a porous nanostructured morphology comprising spherical particles clearly appearing to be more large nano-sized particles (Fig. 7B-C). It was assumed that the mild conditions of the calcination step were not enough to make ripen the grain of calcined dolomite into a larger one size due to sintering, although MgO and La_2O_3-modified calcined dolomite sorbents showed some growth in particle size.

Table 2
Textural properties of freshly and spent sorbents after 40th CaL cycles.

Sample	[a]S_{BET} (m^2g^{-1})	[b]V(cm^3g^{-1})
As-received DOL	0.38	0.002
Freshly calc-DOL	20.0	0.148
Spent calc-DOL	12.2	0.075
As-prepared MgO-calc-DOL	27.5	0.190
Spent MgO-calc-DOL	25.0	0.175
As-prepared LaO-calc-DOL	25.0	0.160
Spent LaO-calc-DOL	22.5	0.145

[a] S_{BET} = specific surface area.
[b] V = Total pore volume measured at a relative pressure (P/P_0) of 0.99.

3.2. Calcium looping performance of samples

In Fig. 8(A-C) are shown the CO_2 uptake performances of freshly calc-DOL, 20MgO-calc-DOL, and LaO-calc-DOL sorbents during three successive CaL cycles at 600 (a) and 700 °C (b) carbonation temperatures under 25 % CO_2 (N_2 balance). The associated exothermic heat flows are also reported. The obtained results will be illustrated in detail below.

3.2.1. Calc-DOL

From the CO_2 uptake/time curves of calc-DOL at both 600 and 700 °C carbonation temperature shown in Fig. 8A(a,b), it can be seen that CaO reactivity towards CO_2 under chemical control regime reached over 90–92 % of its theoretical CO_2 capture capacity in short reaction times (within 40 s). Whereupon the saturation was monotonically established due to the instauration of the diffusion control regime (insets of Fig. 8Aa,b). Although the chemical kinetics of the CaO carbonation reaction is very fast at the beginning of carbonation reaction the network of pores tends to close with the progress of carbonation reaction owing to the large gap in the molar volume between CaO and $CaCO_3$ particles (16.9 and 36.9 cm^3/mol, respectively) [49]. It is supposed that once the $CaCO_3$ product shell reached a thickness between 22 and 90 nm the diffusion-stage was started and the CO_2 diffusion through the shell to reach the inner CaO surface becomes the limiting step [50–52]. Moreover, the complete re-carbonation hardly occurs already in the first carbonation cycle owing to the sintering phenomena during calcination stage at high temperature [50]. The CO_2 absorption capacity was 0.43 and 0.44 $g_{CO_2} \cdot g_{sorbent}^{-1}$ at 600 and 700 °C, respectively, whereas the intensity of the corresponding exothermic heat flow values increased with the enhancement of carbonation temperature (Fig.8Aa,b). It is supposed that the rise of temperature favors the absorption kinetics, but it is limited by the unfavorable effect due to the exothermic nature of the process [53,54].

3.2.2. MgO-calc-DOL

The CO_2 uptake/time curves of MgO-calc-DOL sample show the CO_2 uptake under chemical regime was faster (within 25 s) and steeper with the increasing of carbonation temperature up to 700 °C respect to undoped calcined dolomite (Fig. 8Ba,b). Accordingly, the values of heat flow associated to each CO_2 adsorption cycle indicated higher stability. It was evident that although the CaO conversion values were as high as 94–98 % (insets of Fig. 8B) the CO_2 uptake capacity values were lower

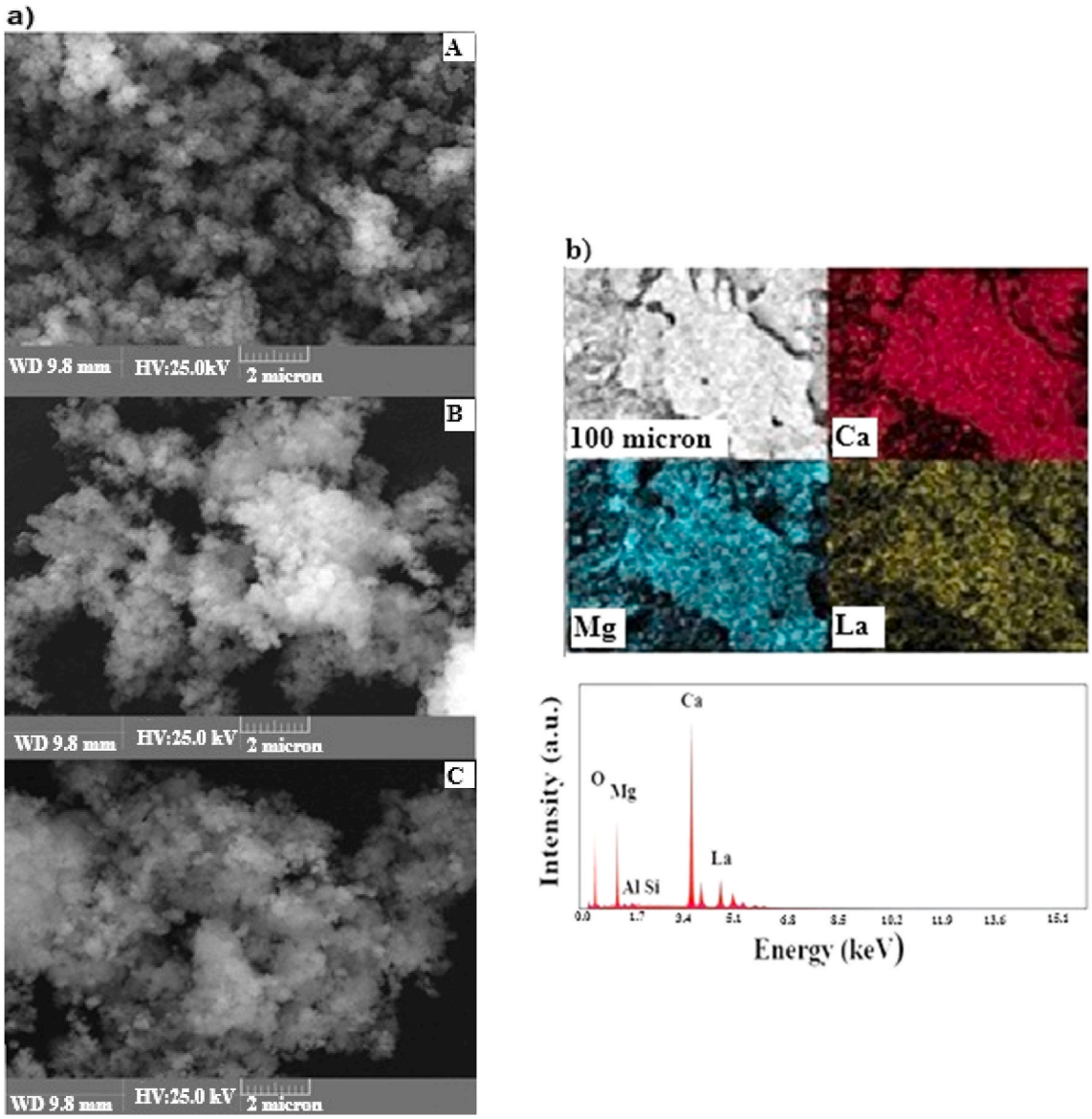

Fig. 6. (a) SEM images of: (A) freshly calc-DOL; as-prepared: (B) MgO-calc-DOL, and (C) LaO-calc-DOL. (b) SEM image, mapping of elements (Ca, Mg, La) and EDS spectrum of as-prepared LaO-calc-DOL.

(0.36–0.37 $g_{CO_2} \cdot g_{sorbent}^{-1}$) due to the low mass fraction of CaO. However, higher CO_2 sorption cyclic stability was observed between the three CaL cycles. It was reported that the mineral huntite ($CaMg_3(CO_3)_4$), where each CaO molecule is surrounded by three MgO molecules, showed higher CO_2 capture capacity and stability compared to natural dolomite [55]. The incorporation of Mg ions into CaO crystal structure can promote stronger Mg-O-Ca interactions favoring electron transfer capacity and oxygen vacancy generation suitable for the reaction of metal oxides with CO_2 [56]. It was evident that the addition of extra MgO into the skeleton of sorbent hinders the particles growth by making easily get the CO_2 gas in contact with the granules of CaO particles. However, the wet chemical preparation method used in the present work allows the mean particle size of the sorbent be small enough, but overall to remain well dispersed during repeated absorption/desorption cycles.

3.2.3. *LaO-calc-DOL*

The CO_2 uptake/time profiles of LaO-calc-DOL sample were distinctly different from those reported for undoped calcined dolomite as depicted in Fig. 8C(a,b), as well the corresponding exothermic heat flows were represented by broader DSC peaks. Meanwhile higher conversion values between 90 and 95 % and CO_2 uptake values of 0.34–0.36 $g_{CO_2} \cdot g_{sorbent}^{-1}$ were reached at longer carbonation times (insets of Fig. 8C(a,b)). Interestingly, the CO_2 adsorption/time curves under kinetic chemical control exhibited two different slopes before diffusion stage started. If the La_2O_3 additive is not considered completely inert to CO_2 it can contribute to the total CO_2 adsorption on calcined dolomite modified with La_2O_3. For this purpose, pure La_2O_3 coming from the calcination of $La(OH)_3$ precursor at 900 °C under N_2 atmosphere was submitted to three CaL cycles at 600 and 700 °C as shown in Fig. 9a,b along with the heat flow profiles. The highest fraction of CO_2 captured was about 90 % (0.119 CO_2 g per gram of La_2O_3) at 700 °C. The insets in Fig. 9 show that the conversion degree during long carbonation time (30 min) was in the first cycle approximately 96 and 98 wt% at 600 and 700 °C, respectively, and remained highly stable after three cycles. These results confirm the substantial positive contribution that the La_2O_3-dopant could bring to the total CO_2 chemical adsorption on calcined dolomite under the current CaL conditions. The uptake rates of LaO-calc-DOL were provided by differentiating the CO_2 absorption curves over time of 1st-3rd CaL cycle at 600 and 700 °C as showed in

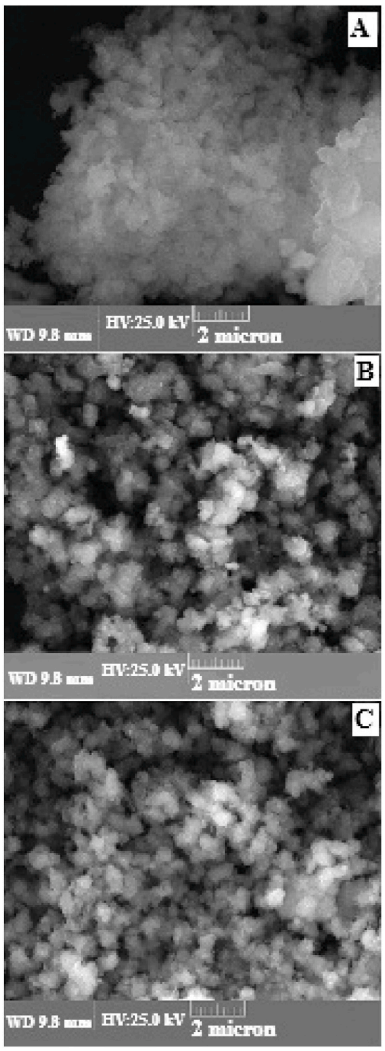

Fig. 7. SEM images of: (A) calc-DOL, (B) MgO-calc-DOL and (C) LaO-calc-DOL after carbonation step of the 3rd CaL cycle at 700 °C under 25 % CO_2 (N_2 balance).

Fig. 10. From Fig. 10a,b it is seen that carbonation reaction rates at both carbonation temperatures quickly increased within 20 s followed by a rapid reduction when the carbonation reaction enters the diffusion regime. However, a second small broad peak slightly overlapping the first one appeared at longer times. Gaussian multi-peak fitting simulation (Origin 8.0 software) applied to the derivative curves of the 1st cycle showed deconvolution of two overlapped peaks with different CO_2 uptake rates. The first peak was centered at about 20 s at both carbonation temperatures, whereas the second less prominent peak was centered at 50 s at 600 °C and 38 s at 700 °C (insets of Fig. 10). It is assumed that the CO_2 capture on calcined dolomite modified with La_2O_3 at first involves the rapid reaction of CO_2 with the surface of CaO particles forming a $CaCO_3$ product layer, on which a second carbonation reaction involving the La_2O_3-dopant is superimposed forming thus $La_2O_2CO_3$. Even though lanthanum trioxide may capture extra CO_2 gas, a $CaCO_3$/$La_2O_2CO_3$ mixed shell could be formed around the CaO particle surface, which could mostly slow down the carbonation reaction rate due to resistance to CO_2 diffusion through two different carbonate layers produced [57].

3.3. Cyclic stability test

Long-term cycle life tests were conducted by submitting all the three sorbents to 40 CaL cycles at carbonation temperatures of both 600 and 700 °C, and the results, expressed as both effective CO_2 conversion and CO_2 uptake capacity in each cycle are shown in Fig. 11. It is observed that the initial conversion values and the CO_2 capture capacity at 600 °C carbonation temperature (Fig. 11a) were lower than those obtained at higher carbonation temperature of 700 °C (Fig. 11b). The cycling stability performances of all three sorbents during the CaL process rapidly decreased with the increasing of cycles number due to the sorbent deactivation. Even more, the calc-DOL sorbent degraded more rapidly than the modified calc-DOL ones, reaching conversions of up to 60–70 % after the 10th cycle. Meanwhile, the conversion degree levelled off at over 92–95 % for MgO-calc-DOL and almost 83–88 % for LaO-calc-DOL after the 10th cycle, regardless of the carbonation temperature. Although the theoretical CO_2 capture capacity of calc-DOL is higher than that of modified calc-DOL due to the higher mass fraction of CaO in the sample, after the conversions level out the CO_2 capture capacities were higher than undoped calcined dolomite. In terms of effective CO_2 uptake capacity the results were 0.28, 0.35, and 0.30 $g_{CO_2} \cdot g_{sorbent}^{-1}$ at 600 °C and 0.32, 036, and 0.33 $g_{CO_2} \cdot g_{sorbent}^{-1}$ at 700 °C for calc-DOL, MgO-calc-DOL, and LaO-calc-DOL, respectively. The CO_2 capture capacity of the MgO-doped calcined dolomite remained highly stable over the entire number of cycles owing to the anti-sintering effect. While the LaO-calc-DOL with the La_2O_3 additive having a $T_{Tammann}$ of around 1021 °C (≈half of the melting temperature on the Kelvin scale) had a good influence in terms of cyclic stability compared to undoped dolomite, which decreased more rapidly after the first ten cycles. Indeed, the La_2O_3 addition in calc-DOL caused a decrease of the average crystal size of CaO and an enhancement of S_{BET} compared to undoped calcined dolomite. As showed in Fig. 11 after 10th CaL cycle the cycles reached a good stability at both carbonation temperature. The La_2O_3-dopant could be involved in the carbonation reaction giving its contribution to the total CO_2 adsorption capacity of the sorbent. However, the effective advantage of pretreatment of CaO lime or calcined dolomite with La_2O_3 dopant to increase its CO_2 capture capacity and stability over cycling could be ascribed to sintering/agglomeration inhibitory effect, which will mainly depend upon both the preparation method [21,28] and the kind of lanthanum trioxide precursor used [58].

3.4. CO_2 uptake kinetics

Kinetic analysis of carbonation reaction of all three sorbents was conducted by applying the classical grain model (GM) for non-catalytic gas-solid reaction in porous media [59]. This model has been widely used in the past by several authors to model the carbonation reaction because of its simplicity in requiring minimal calculations in the acquisition of the main physical-chemical parameters [60]. Although the model is not longer applicable in the CO_2 diffusion regime owing to the clogging of pores of produced $CaCO_3$, the grain model has provide an appropriate description of the progress of carbonation reaction with time [61]. Under kinetic control, the specific reaction rate of CaO carbonation is defined as CaO conversion X *vs* time derivative divided per $(1\text{-}(1\text{-}X))^{2/3}$ according to the following equation [62]:

$$\frac{dX}{dt(1-(1-X))^{2/3}} = 3k \tag{7}$$

where k is the intrinsic surface reaction rate constant (s^{-1}).

In integral form:

$$\left[1-(1-X)^{1/3}\right] = k_s t \tag{8}$$

Eq. (8) shows that when the reaction is under kinetic control, the plot of $[1 - (1 - X)]^{1/3}$ *vs* t should give a straight line with the slope being k. In Fig. 12 are reported the linear part of the carbonation conversion curves at the 1st CaL cycle at two different carbonation temperatures for all three sorbents. At the beginning of carbonation reaction there was an

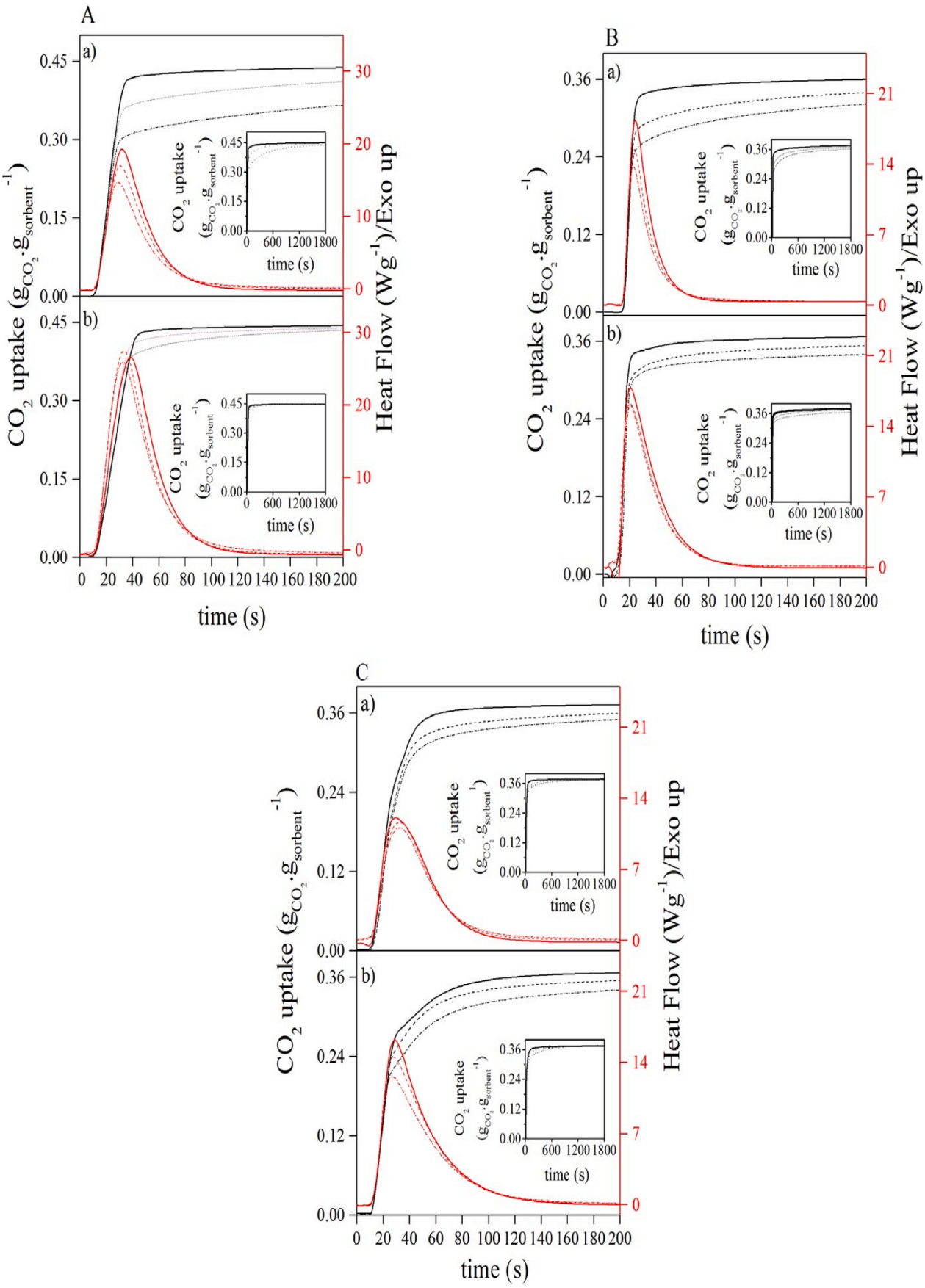

Fig. 8. CO_2 uptake *vs* time (insets: measured data within 1800 s) of cal-DOL (A), MgO-calc-DOL (B), and LaO-calc-DOL (C) at both 600 °C (a) and 700 °C (b) under 25 % CO_2 (N_2 balance) along with the associated exothermic heat flows at three different cycles: 1st (–); 2nd (–); and 3rd (-· -).

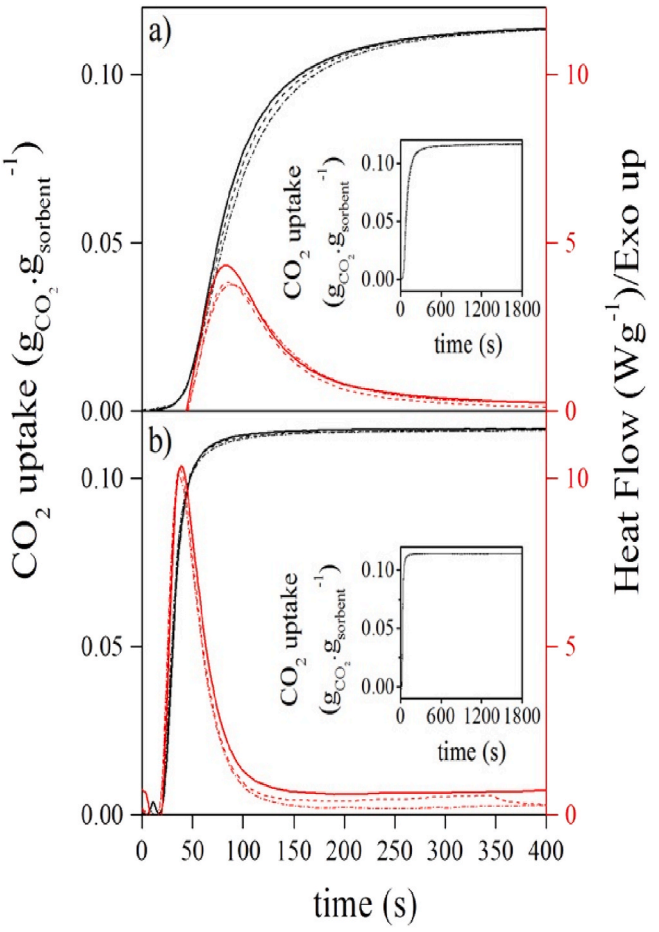

Fig. 9. CO_2 uptake *vs* time (insets: measured data within 1800 s) of pure La_2O_3 at both 600 °C (a) and 700 °C (b) under 25 % CO_2 (N_2 balance) along with the associated exothermic heat flows at three different cycles: 1st (–); 2nd (–); and 3rd (-· -).

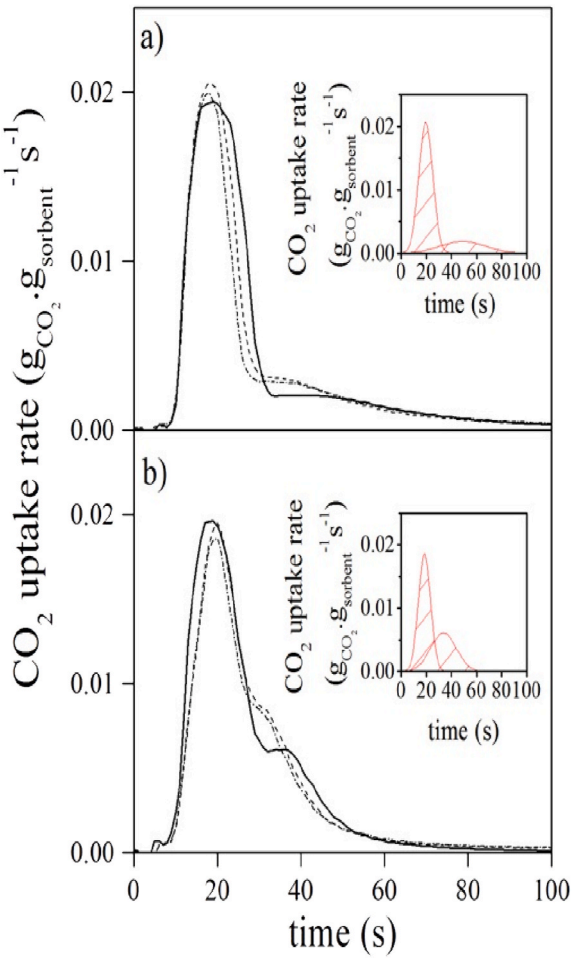

Fig. 10. CO_2 uptake rate *vs* time of LaO-calc-DOL at both 600 °C (a), and 700 °C (b) under 25 % CO_2 (N_2 balance) at three different cycles: 1st (–); 2nd (–); and 3rd (-· -). Insets: deconvolution peaks of CO_2 uptake rate at 1st CaL cycle.

initial induction period where the slopes of the curves are equal to zero. Therefore, the kinetic results were normalized at $t = t^* + t_0$ where t_0 is the time at which carbonation initiate [62]. From Fig. 12 can be seen that calcined dolomite presented almost the same initial induction time at both 600 and 700 °C carbonation temperatures, but different slopes of the linear portion. When an extra 20 %wt. MgO is added to calcined dolomite a more pronounced transition from kinetic regime to diffusion one was clearly emphasized, while the initial induction period occurred earlier at the carbonation temperature of 700 °C. The effect of addition of extra MgO to calcined dolomite is reflected in a deeply increase in the carbonation rate at higher temperatures due to changes in structural and textural features. Conversely, in the chemical kinetic regime, La_2O_3--modified calcined dolomite exhibited slightly different slopes before the diffusion regime was established. In Table 3 are reported the intrinsic surface reaction rate constant values k calculated from the linear portion of conversion by classical model obtained over 1st CaL cycle at two different carbonation temperatures for all three sorbents. The correlation coefficients R^2 of the linear regression fits, which were better than 0.99, were also reported in Table 3. The obtained k values were in accordance with that reported in literature [63]. As it can be seen, MgO-modified calcined dolomite presented the largest values of k, almost three times the intrinsic rate constant values of both La_2O_3-modified calcined dolomite and unmodified calcined dolomite.

The specific rate of the carbonation reaction can be expressed in power law form, which relates the variation of X conversion over time to the P_{CO_2} and to the power of the reaction order n as follows [63]:

$$R = \frac{dX}{dt(1-(1-X))^{2/3}} = 3k = 56k_s\left(P_{CO_2} - P_{CO_2,eq}\right)^n S \tag{9}$$

where 56 is the molar weight ($g \cdot mol^{-1}$) of CaO, S the specific surface area (m^2/g), and k_s is the intrinsic surface reaction rate constant, which is related to the Arrhenius-type law as follows:

$$k_s = kexp\left(-E_a/RT\right) \tag{10}$$

Where k is the pre-exponential factor (s^{-1}), E_a energy of activation ($J \cdot mol^{-1}$), R is the universal constant of gas (8.314 J mol^{-1} K^{-1}) and T (K) is the absolute temperature of carbonation. Combining equation (10) with equation (9) and assuming reaction order n equal zero when $P_{CO_2} - P_{CO_2,eq}$ >10 kPa it can be obtained the following relation [64]:

$$\ln(r_0) = \ln\left(\frac{56}{3}AS_0\right) - \frac{E_a}{RT} \tag{11}$$

where r_0 (s^{-1}) is the initial specific reaction rate in the carbonation reaction and S_0 ($m^2 \cdot g^{-1}$) is the initial specific surface area, and A ($mol \cdot m^{-2} s^{-1}$) the pre-exponential factor. As showed in Fig. 13, a good linear relationship between $\ln(r_0)$ and 1/T is observed in the temperature range 600–700 °C. Linear fits was performed by least-square method, and from the slopes and intercepts of the linear fits, an estimate of the E_a and the pre-exponential factor, respectively, can be

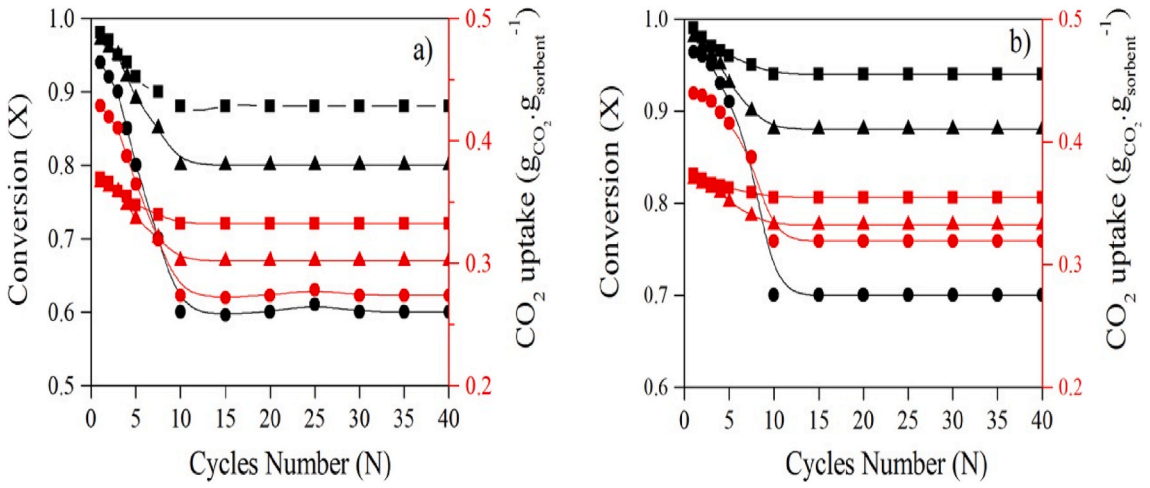

Fig. 11. Conversion (black colour) and CO_2 uptake (red colour) in long-term cycle life tests of calc-DOL (circle), MgO-calc-DOL (square), and LaO-calc-DOL (triangle) at both 600 (a) and 700 °C (b) under 25 %CO_2 (N_2 balance).

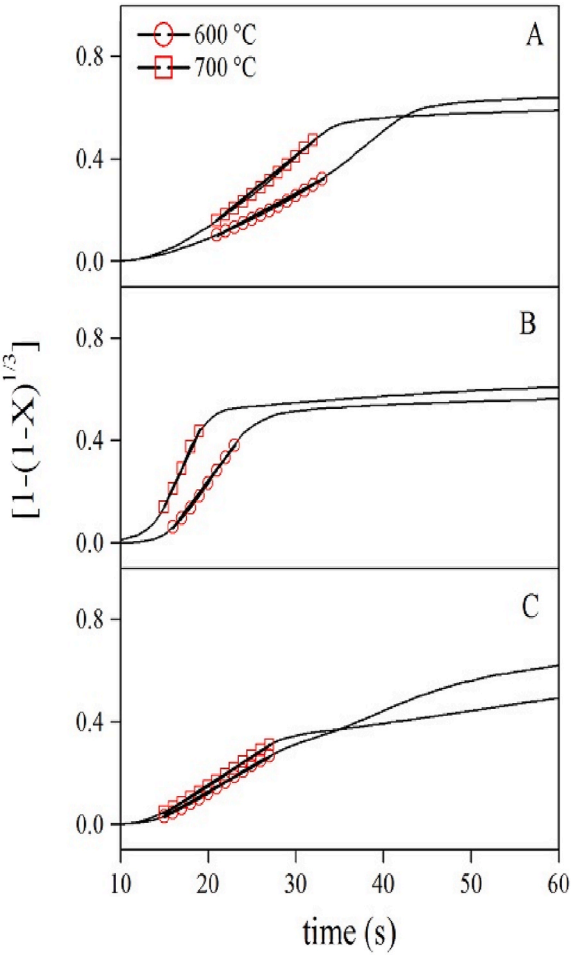

Fig. 12. Conversion by classical grain model for (A) calc-DOL, (B) MgO-calc-DOL, and (C) LaO-calc-DOL in the 1st CaL cycle at both 600 and 700 °C under 25 % CO_2 (N_2 balance) at 1st cycle.

derived as listed in Table 4. In the kinetics controlled-regime the E_a = 35.1 kJmol^{-1} and A = 0.15·10^{-3} mol m^{-2} s^{-1} for calc-DOL were calculated, which were in reasonable agreement with the literature data under similar reaction conditions [64,65]. The activation energy and pre-exponential factor were significantly diminished after doping with

Table 3
Summary of intrinsic rate constants and regression (R^2) of equation (8) for different sorbents from 1st CaL cycle data at both 600 and 700 °C carbonation temperature.

Sample	k (s^{-1})	R^2
calc-DOL		
600 °C	0.0151	0.992
700 °C	0.0210	0.994
MgO-calc-DOL		
600 °C	0.0452	0.996
700 °C	0.0685	0.990
LaO-calc-DOL		
600 °C	0.0201	0.999
700 °C	0.0221	0.996

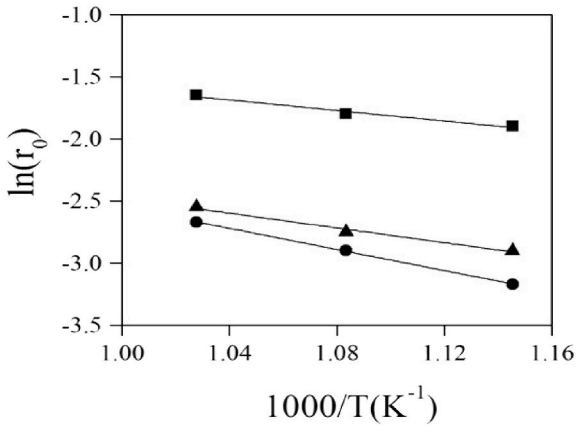

Fig. 13. Arrhenius plots for cal-DOL (•), MgO-cal-DOL (■) and LaO-cal-DOL (▲) under carbonation reaction.

Table 4
Activation energy (E_a), pre-exponential factor (A), and R^2 of different sorbents.

Sample	Ea (kJ·mol^{-1})	A (mol·m^{-2}·s^{-1})	R^2
calc-DOL	35.1	0.15·10^{-3}	0.99
MgO-calc-DOl	18.1	4.5·10^{-3}	0.99
LaO-calc-DOL	24.6	5.6·10^{-3}	0.99

MgO and La_2O_3 to a level of $E_a = 18.1$ kJ·mol^{-1}and A = 4.5·10^{-3} mol m^{-2} s^{-1} and $E_a = 24.6$ kJ·mol^{-1}and A = 5·6·10^{-3} mol m^{-2} s^{-1}, respectively. It is supposed that the inert barrier capacity of both MgO and La_2O_3, which is reflected in a decrease of activation energy of the two doped calcined dolomites, may be due to the effectiveness of the preparation method used to prevent CaO agglomeration. But for the La_2O_3 additive the capacity of capturing CO_2 forming $La_2O_2CO_3$ make it competitive to CaO and the formation of two carbonate layer could be negative in successive cycles [57].

4. Conclusions

Doped calcined dolomites with 20 %wt.MgO or 20 %wt.La_2O_3 were prepared by a simple wet chemical mixing method followed by air-calcination at 900 °C and investigated as solid sorbents for CO_2 capture by TG/DTG/DSC analysis. Apart the higher initial CO_2 capture capacity of undoped dolomite, after the 10th CaL cycle the doped calcined dolomites presented higher CO_2 capture capacities and stability over 40 multiple carbonation(600–700 °C)/calcination(900 °C) cycles owing to the minor deactivation degree respect to undoped one. The incorporation of additives promoted high sintering resistance and CO_2 uptake stability due to the favorable developed structure with smaller CaO crystallite size. Additionally, the La_2O_3 doping of calcined dolomite ameliorated the CO_2 capture capacity by the further CO_2 absorption on La_2O_3 additive, which formed stable and reversible $La_2O_2CO_3$.

CRediT authorship contribution statement

Silvera Scaccia: Writing – review & editing, Writing – original draft, Investigation, Formal analysis, Conceptualization. **Livia Della Seta:** Investigation, Formal analysis. **Daniele Mirabile Gattia:** Investigation, Formal analysis.

Declaration of competing interest

The authors declare that they have no known competing financial interests or personal relationships that could have appeared to influence the work reported in this paper.

Data availability

The authors do not have permission to share data.

References

[1] H. Sun, C. Wu, B. Shen, X. Zhang, Y. Zhang, J. Huang, Progress in the development and application of CaO-based adsorbents for CO_2 capture-a review, Mater. Today Sustain. 1 (2018) 1–27, https://doi.org/10.1016/j.mtsust.2018.08.001.

[2] P. Zang, J. Tang, X. Zhang, L. Cui, J. Chen, P. Zhao, Y. Dong, Strategies to improve CaO absorption cycle stability and progress of catalysts in Ca-based DFMs for integrated CO_2 capture-conversion: a critical review, J. Environ. Chem. Eng. (2023) 111047, https://doi.org/10.1016/j.jece.2023.111047.

[3] A. Perejòn, L.M. Romeo, Y. Lara, P. Lisbona, A. Martinez, J.M. Valverde, The calcium-looping technology for CO_2 capture: on the important roles of energy integration and sorbent behavior, Appl. Energy 162 (2016) 787–807, https://doi.org/10.1016/j.apenergy.2015.10.121.

[4] A.A. Khosa, T. Xu, B.Q. Xia, J. Yan, C.Y. Zhao, Technological challenges and industrial applications of $CaCO_3$/CaO based thermal energy storage system–A review, Sol. Energy 193 (2019) 618–636, https://doi.org/10.1016/j.solener.2019.10.003.

[5] S. Tian, F. Yan, Z. Zhang, J. Jiang, Calcium-looping reforming of methane realizes in situ CO_2 utilization with improved energy efficiency, Sci. Adv. 5 (2019) eaav5077, https://doi.org/10.1126/sciadv.aav5077.

[6] Y. Wang, Y. Li, Sorption-enhanced steam gasification of biomass for H_2-rich gas production and in-situ CO_2 capture by CaO-based sorbents: a critical review, Appl. Energy Combus. Sci. 14 (2023) 100124, https://doi.org/10.1016/j.jaecs.2023.100124.

[7] R. Barker, The reversibility of the reaction $CaCO_3 \leftrightarrow CaO + CO_2$, J. Appl. Chem. Biotechnol. 23 (1973) 733–744, https://doi.org/10.1002/jctb.5020231005.

[8] J. Blamey, E.J. Anthony, J. Wang, P.S. Fennell, The calcium looping cycle for large-scale CO_2 capture, Prog. Energy Combust. Sci. 36 (2010) 260–279, https://doi.org/10.1016/j.pecs.2009.10.001.

[9] J.M. Valverde, P.E. Sanchez-Jimenez, L.A. Perez-Maqueda, High and stable CO_2 capture capacity of natural limestone at Ca-looping conditions by heat pretreatment and re-carbonation synergy, Fuel 123 (2014) 79–85, https://doi.org/10.1016/j.fuel.2014.01.045.

[10] Y. Hu, W. Liu, J. Sun, M. Li, X. Yang, Y. Zhang, X. Liu, M. Xu, Structurally improved CaO-based sorbent by organic acids for high temperature CO_2 capture, Fuel 167 (2016) 17–24, https://doi.org/10.1016/j.fuel.2015.11.048.

[11] R. Han, Y. Wang, S. Xing, C. Pang, Y. Hao, C. Song, Q. Liu, Progress in reducing calcination reaction temperature of Calcium-looping CO_2 capture technology: a critical review, Chem. Eng. J. 450 (2022) 137952, https://doi.org/10.1016/j.cej.2022.137952.

[12] Y. Hu, H. Lu, W. Liu, Y. Yang, H. Li, Incorporation of CaO into inert supports for enhanced CO_2 capture: a review, Chem. Eng. J. 396 (2020) 125253, https://doi.org/10.1016/j.cej.2020.125253.

[13] M.T. Dunstan, F. Donat, A.H. Bork, C.P. Grey, C.R. Müller, CO_2 capture at medium to high temperature using solid oxide-based sorbents: fundamental aspects, mechanistic insights, and recent advances, Chem. Rev. 121 (2021) 12681–12745, https://doi.org/10.1021/acs.chemrev.1c00100.

[14] L. Tao, J. Huang, D. Dastan, T. Wang, J. Li, X. Yin, Q. Wang, New insight into absorption characteristics of CO_2 on the surface of calcite, dolomite, and magnesite, Appl. Surf. Sci. 540 (2021) 148320, https://doi.org/10.1016/j.apsusc.2020.148320.

[15] M.W. Islam, A review of dolomite catalyst for biomass gasification tar removal, Fuel 267 (2020) 117095, https://doi.org/10.1016/j.fuel.2020.117095.

[16] M.A. Carreon, V.V. Guliants, Ordered meso-and macroporous binary and mixed metal oxides, Eur. J. Inorg. Chem. 1 (2005) 27–43, https://doi.org/10.1002/ejic.200400675.

[17] K. Wang, D. Han, P. Zhao, X. Hu, Z. Yin, D. Wu, Role of $Mg_xCa_{1-x}CO_3$ on the physical-chemical properties and cyclic CO_2 capture performance of dolomite by two-step calcinations, Thermochim. Acta 614 (2015) 199–206, https://doi.org/10.1016/j.tca.2015.06.033.

[18] M. Broda, A.M. Kierzkowska, C.R. Müller, Development of highly effective CaO-based, MgO-stabilized CO_2 sorbents via a scalable "one-pot" recrystallization technique, Adv. Funct. Mater. 24 (2014) 5753–5761, https://doi.org/10.1002/adfm.201400862.

[19] H. Guo, Z. Xu, T. Jiang, Y. Zhao, X. Ma, S. Wang, The effect of incorporation Mg ions into the crystal lattice of CaO on the high temperature CO_2 capture, J. CO2 Util. 37 (2020) 335–345, https://doi.org/10.1016/j.jcou.2020.01.012.

[20] L. Huang, Q. Zheng, B. Louis, Q. Wang, A facile solvent/nonsolvent preparation of sintering-resistant MgO/CaO composites for high-temperature CO_2 capture, Energy Technol. 6 (2018) 2469–2478, https://doi.org/10.1002/ente.201800300.

[21] K.O. Albrecht, K.S. Wagenbach, J.A. Satrio, B.H. Shanks, T.D. Wheelock, Development of a CaO-Based CO_2 sorbent with improved cyclic stability, Ind. Eng. Chem. Res. 47 (2008) 7841–7848, https://doi.org/10.1021/ie8007743.

[22] R. Filitz, A.M. Kierzkowska, M. Broda, C.R. Müller, Highly efficient CO_2 sorbents: development of synthetic, calcium-rich dolomites, Environ. Sci. Technol. 46 (2012) 559–565, https://doi.org/10.1021/es2034697.

[23] W. Liu, B. Feng, Y. Wu, G. Wang, J. Barry, J.C. Diniz da Costa, Synthesis of sintering-resistant sorbents for CO_2 capture, Environ. Sci. Technol. 44 (2010) 3093–3097, https://doi.org/10.1021/es903436v.

[24] Q. Zhu, S. Zeng, Y. Yu, A model to stabilize CO_2 uptake capacity during carbonation–calcination cycles and its case of CaO-MgO, Environ. Sci. Technol. 51 (2017) 552–559, https://doi.org/10.1021/acs.est.6b04100.

[25] K. Wang, X. Hu, P. Zhao, Z. Yin, Natural dolomite modified with carbon coating for cyclic high-temperature CO_2 capture, Appl. Energy 165 (2016) 14–21, https://doi.org/10.1016/j.apenergy.2015.12.071.

[26] R. Han, S. Xing, X. Wu, C. Pang, S. Lu, Y. Su, Q. Liu, C. Song, J. Gao, Relevant influence of alkali carbonate doping on the thermochemical energy storage of Ca-based natural minerals during CaO/$CaCO_3$ cycles, Renew. Energy 181 (2022) 267–277, https://doi.org/10.1016/j.renene.2021.09.021.

[27] L. Di Felice, C. Courson, P.U. Foscolo, A. Kiennemann, Iron and nickel doped alkaline-earth catalysts for biomass gasification with simultaneous tar reformation and CO_2 capture, Int. J. Hydrogen Energy 36 (2011) 5296–5310.

[28] S. Bai, J. Sun, L. Liu, Y. Da, Z. Zhou, R. Wang, Y. Guo, C. Zhao, Dolomite-derived composites doped with binary ions for direct solar thermal conversion and stabilized thermochemical energy storage, Sol. Energy Mater. Sol. Cell. 239 (2022) 111659, https://doi.org/10.1016/j.solmat.2022.111659.

[29] A. Moral, A.C. Wold, K.R. Rout, D. Chen, Modified dolomite-based pellets for high temperature post-combustion CO_2 capture, in: 11th International Trondheim CCS Conference. CO_2 Capture, Transport and Storage, SINTEF Academic Press, Trondheim, 2021, 22nd–23rd June.

[30] C. Luo, Y. Zheng, N. Ding, Q. Wu, G. Bian, C. Zheng, Development and performance of CaO/La_2O_3 sorbents during calcium looping cycles for CO_2 capture, Ind. Eng. Chem. Res. 49 (2010) 11778–11784, https://doi.org/10.1021/ie1012745.

[31] C. Luo, Y. Zheng, N. Ding, C. Zheng, Enhanced cyclic stability of CO_2 adsorption capacity of CaO-based sorbents using La_2O_3 or $Ca_{12}Al_{14}O_{33}$ as additives, Kor. J. Chem. Eng. 28 (2011) 1042–1046, https://doi.org/10.1007/s11814-010-0469-z.

[32] S. Becker, M. Baerns, Oxidative coupling of methane over La_2O_3-CaO catalysts effect of bulk and surface properties on catalytic performance, J. Catal. 128 (1991) 512–519, https://doi.org/10.1016/0021-9517(91)90308-Q.

[33] A.N. Shirsat, M. Ali, K.N.G. Kaimal, S.R. Bharadwaj, D. Das, Thermochemistry of $La_2O_2CO_3$ decomposition, Thermochim. Acta 399 (2003) 167–170, https://doi.org/10.1016/S0040-6031(02)00459-8.

[34] N. Afandi, M. Satgunam, S. Mahalingam, A. Manap, F. Nagi, W. Liu, R.B. Johan, A. Turan, A. W-Y Tan, S. Yunus, Review on the modifications of natural and industrial waste CaO based sorbent of calcium looping with enhanced CO_2 capture

capacity, Heliyon 10 (2024) e27119, https://doi.org/10.1016/j.heliyon.2024.e27119.
[35] Q. Zhu, S. Zeng, Y. Yu, A model to stabilize CO_2 uptake capacity during carbonation-calcination cycles and its case of CaO-MgO, Environ. Sci. Technol. 51 (2017) 552–559, https://doi.org/10.1021/acs.est.6b04100.
[36] M.J. Al-Jeboori, P.S. Fennell, M. Nguyen, K. Feng, Effects of different dopants and doping procedures on the reactivity of CaO-based sorbents for CO_2 capture, Energy Fuels 26 (2012) 6584–6594, https://doi.org/10.1021/ef301153b.
[37] J. Phromprasit, J. Powell, S. Assabumrungrat, Metals (Mg, Sr and Al) modified CaO based sorbent for CO_2 sorption/desorption stability in fixed bed reactor for high temperature application, Chem. Eng. J. 284 (2016) 1212–1223, https://doi.org/10.1016/j.cej.2015.09.038.
[38] Z. Xu, T. Jiang, H. Zhang, Y. Zhao, X. Ma, S. Wang, Efficient MgO-doped CaO sorbent pellets for high temperature CO_2 capture, Front. Chem. Sci. Eng. 15 (2021) 698–708, https://doi.org/10.1007/s11705-020-1981-2.
[39] C. Ortiz, J.M. Valverde, R. Chacartegui, L.A. Pérez-Maqueda, P. Gimenez-Gavarrell, Scaling-up the calcium-looping process for CO_2 capture and energy storage,, KONA Powder Particle J. 38 (2021) 189–208, https://doi.org/10.14356/kona.2021005.
[40] P. Scherrer, Bestimmung dergrosse und der inneren struktur yon kolloiteilchen mittels, Gott. Nachr Math. Phys 2 (1918) 98–100.
[41] S. Gunasekaran, G. Anbalagan, Spectroscopic study of phase transitions in dolomite mineral, J. Raman Spectrosc. 38 (2007) 846–852, https://doi.org/10.1002/jrs.1718.
[42] F. Rouquerol, J. Rouquerol, K. Sing, in: Eds, in: F. Rouquerol, J. Rouquerol, K. Sing (Eds.), Adsorption by Powders and Porous Solids, vol. 11, Academic Press, San Diego, 1999.
[43] M.B. Kruger, Q. Williams, R. Jeanloz, Vibrational spectra of $Mg(OH)_2$ and $Ca(OH)_2$ under pressure, J. Chem. Phys. 91 (1989) 5910–5915, https://doi.org/10.1063/1.457460.
[44] J.M. Valverde, A. Perejon, S. Medina, L.A. Perez-Maqueda, Thermal decomposition of dolomite under CO_2: insights from TGA and in situ XRD analysis, Phys. Chem. Chem. Phys. 17 (2015) 30162–30176, https://doi.org/10.1039/C5CP05596B.
[45] A. Silaban, M. Narcida, D.P. Harrison, Characteristics of the reversible reaction between CO_2(g) and calcined dolomite, Chem. Eng. Commun. 146 (1996) 149–162, https://doi.org/10.1080/00986449608936487.
[46] M. Imani, M. Tahmasebpoor, P.E. Sánchez-Jiménez, Metal-based eggshell particles prepared via successive incipient wetness impregnation method as a promoted sorbent for CO_2 capturing in the calcium looping process, J. Environ. Chem. Eng. 11 (2023) 110584, https://doi.org/10.1016/j.jece.2023.110584.
[47] F. Rubiera, A.B. Fuertes, J.J. Pis, V. Artos, G. Marban, Changes in textural properties of limestone and dolomite during calcination, Thermochim. Acta 179 (1991) 125–134, https://doi.org/10.1016/0040-6031(91)80341-F.
[48] J.C. Maya, F. Chejne, C.A. Gómez, S.K. Bhatia, Effect of the CaO sintering on the calcination rate of $CaCO_3$ under atmospheres containing CO_2, AIChE J. 64 (2018) 3638–3648, https://doi.org/10.1002/aic.16326.
[49] S.K. Bhatia, D.D. Perlmutter, Effect of the product layer on kinetics of the CO_2-lime reaction, AIChE J. 29 (1983) 79–86, https://doi.org/10.1002/aic.690290111.
[50] D. Alvarez, J.C. Abanades, Determination of the critical product layer thickness in the reaction of CaO and CO_2, Ind. Eng. Chem. Res. 44 (2005) 5608–5615, https://doi.org/10.1021/ie050305s.
[51] H. Sun, J. Wang, X. Liu, B. Shen, C.M.A. Parlett, G.O. Adwek, E.J. Anthony, P. T. Williams, C. Wu, Fundamental studies of carbon capture using CaO-Based materials, J. Mater. Chem. A 7 (2019) 9977–9987, https://doi.org/10.1039/C8TA10472G.
[52] D.Y. Lu, R.W. Hughes, E.J. Anthony, V. Manovic, Sintering and reactivity of $CaCO_3$-based sorbents for in situ CO_2 capture in fluidized beds under realistic calcination conditions, J. Environ. Eng. 135 (2009) 404–410, https://doi.org/10.1061/(ASCE)EE.1943-7870.0000079.
[53] P. Lan, S. Wu, Mechanism of self-reactivation of nano-cao-based CO_2 sorbent in calcium looping, Fuel 143 (2015) 9–15, https://doi.org/10.1016/j.fuel.2014.11.004.
[54] G. Ji, H. Yang, M.Z. Memon, Y. Gao, B. Qu, W. Fu, G. Olguin, M. Zhao, A. Li, Recent advances on kinetics of carbon dioxide capture using solid sorbents at elevated temperatures, Appl. Energy 267 (2020) 114874, https://doi.org/10.1016/j.apenergy.2020.114874.
[55] A. Bandi, M. Specht, P. Sichler, N. Nicoloso, In Situ Gas Conditioning in Fuel Reforming for Hydrogen Generation In: 5Th International Symposium on Gas Cleaning at High Temperature, US DOE National Energy Technology Laboratory, Morgantown, USA, 2002.
[56] X. Yang, L. Zhao, S. Yang, Y. Xiao, Investigation of natural CaO-MgO sorbent for CO_2 capture, Asia-Pacific, J. Chem. Eng. 8 (2013) 906–915, https://doi.org/10.1002/apj.1735.
[57] E. Wang, R. Li, Z. Zhu, J. Wu, K. Ma, J. Zhang, A novel core-shell (CaO/La_2O_3)@La_2O_3 composite adsorbent for high temperature calcium cycling CO_2 capture based on skeleton stabilization effect: an experimental and DFT stud, Fuel 388 (2025) 134506, https://doi.org/10.1016/j.fuel.2025.134506.
[58] S.A. Salaudeen, B. Acharya, A. Dutta, CaO-based CO_2 sorbents: a review on screening, enhancement, cyclic stability, regeneration and kinetics modelling, J. CO2 Util. 23 (2018) 179–199, https://doi.org/10.1016/j.jcou.2017.11.012.
[59] J. Szekely, J.W. Evans, H.Y. Sohn, Gas Solid Reactions, Academic Press, London, 1976.
[60] Y.C. García I- Martínez, G. Grasa, Determination of the hydration and carbonation kinetics of CaO for low-temperature applications, Chem. Eng. Sci. 295 (2024) 120146, https://doi.org/10.1016/j.ces.2024.120146.
[61] Z. Li, General rate equation theory for gas–solid reaction kinetics and its application to CaO carbonation, Chem. Eng. Sci. 227 (2020) 115902, https://doi.org/10.1016/j.ces.2020.115902.
[62] P. Sun, J.R. Grace, C.J. Lim, E.J. Anthony, Determination of intrinsic rate constants of the CaO–CO_2 reaction, Chem. Eng. Sci. 63 (2008) 47–56, https://doi.org/10.1016/j.ces.2024.120146.
[63] R.T. Symonds, D.Y. Lu, A. Macchi, R.W. Hughes, E.J. Anthony, CO_2 capture from syngas via cyclic carbonation/calcinations for a naturally occurring limestone: modelling and bench-scale testing, Chem. Eng. Sci. 64 (2009) 3536–3543, https://doi.org/10.1016/j.ces.2009.04.043.
[64] D.K. Lee, An apparent kinetic model for the carbonation of calcium oxide by carbon dioxide, Chem. Eng. J. 100 (2004) 71–77, https://doi.org/10.1016/j.cej.2003.12.003.
[65] Z.S. Li, F. Fang, X.Y. Tang, N.S. Cai, Effect of temperature on the carbonation reaction of CaO with CO_2, Energy Fuels 26 (2012) 2473–2482, https://doi.org/10.1021/ef201543n.